Direct correlation functions in two-dimensional anisotropic fluids

Antoine Chamoux and Aurelien Perera
Laboratoire de Physique Théorique des Liquides, Université Pierre et Marie Curie, 4 Place Jussieu, 75252 Paris Cedex 05, France*
(Received 13 February 1998)

A geometrical approximation for the direct correlation of two-dimensional multicomponent fluids is introduced herein. This approximation is semianalytical and involves the knowledge of elementary geometrical properties of a single particle. The formalism is applied to anisotropic two-dimensional fluids of various particle shapes such as hard ellipses, diskorectangles, and cut disks of various size ratios. The particular case of the hard needles fluid is also investigated. The accuracy of the approximation is tested by comparing the equation of state and the correlation functions to those obtained by integral equation techniques and Monte Carlo simulations. In almost all cases these comparisons are found to be quite satisfactory and even excellent in the case of moderate size ratios. Both the isotropic and orientationally ordered phases are investigated and particular attention is paid to the orientational stability of the isotropic phase. The cut disk fluid has a particularly interesting long-range order for thicknesses around 0.3, which is very much reminiscent of the *cubatic* order observed in the corresponding three-dimensional case of cut spheres. This feature observable by both the simulations and the hypernetted chain integral equation is also predicted by the present geometrical theory, but at larger thicknesses. [S1063-651X(98)07408-X]

PACS number(s): 61.20.−p, 61.30.−v, 64.70.Ja, 68.15.+e

I. INTRODUCTION

Many thin films of liquid crystalline substances form quasi-idealized two-dimensional liquid crystalline phases [1]. If one concentrates solely on the interactions based on steric considerations, which is quite reasonable for these molecules, which are mostly rodlike, then one can resort to two-dimensional convex shapes in order to model such fluids. This simplification certainly captures the essential of the excluded volume interaction contribution to the physics of such fluids. This is the point of view we adopt here by considering two-dimensional fluids made of several hard convex shapes such as ellipses, diskorectangles (made of two half disks encapsulating a rectangle), which are the two-dimensional equivalent of the spherocylinders, and cut disks (a disk from which two equal caps have been removed from top and bottom), which are similar to the cut spheres in three dimensions. These simple shapes can be described with few parameters such as the aspect ratio for the ellipse, the diameter σ of the disk, the length of the cylinder L in the case of the diskorectangle, and the thickness of the cut disk d. Unlike the hard disk fluid, which has been abundantly studied in the past by both computer simulations and various standard theories of liquids, other convex shapes have received little attention. A notable exception is the hard ellipse liquid, which has been studied by computer simulations [2], density functional theories [3], and integral equation methods [4,5].

Although being simple models of two-dimensional liquid crystalline phases, the hard ellipse fluids have surprisingly interesting properties. The computer simulations have revealed that for aspect ratios large enough to give a liquid crystalline phase (about 4) the isotropic-nematic transition was, as expected, second order for large aspect ratios (about 6), but *first* order for smaller ones. The study of phase transitions in two-dimensional systems is still full of controversies. For example, the question about the order of the fluid-solid transition of the hard disk fluid is still unanswered [6,7] (one first-order transition or two second-order transitions via a hexatic phase). The basic mechanism for the transition in two dimensions is based on the unbinding of defects formed in the ordered phase, following a Kosterlitz-Thouless [8] type of scenario. The detection of such transition by finite size computer simulation techniques is not straightforward [2]. It is not the aim of the present work, however, to get into such considerations. Rather, the focus is on standard equilibrium theory of liquids, more precisely, the determination of the equation of state (EOS) and the structural features of the isotropic phase.

An essential ingredient of the theory of fluid is the direct correlation function (DCF), which allows the determination of the mechanical stability (the compressibility) and the orientational stability (the Kerr constant) of the fluid, as well as the pair correlation function to which it is linked by the Ornstein-Zernike equation [9]. Unlike the pair correlation function, which has a physical meaning and can be measured by computer simulations, the direct correlation function has only a formal definition relating it to the second-order functional derivative of the free energy [9]. The Percus-Yevick analytical solution in the case of the hard spheres and mixtures is not much help in this matter. Such a solution is not known for even dimensions [10]. Recently, Rosenfeld [11] has put forth an illuminating geometrical interpretation of the Percus-Yevick solution for the case of hard spheres that allows one to express the direct correlation function as a separable function of density and various geometrical functions of the overlap between two hard spheres. The most appealing feature of this formalism is that these geometrical functions are expressed solely in terms of various weight functions depending on the individual molecular geometrical properties. Rosenfeld also proposed an extension to two dimensions

*Unité associée au CNRS.

[12], obtaining an analytical expression for the DCF for hard disks and mixtures.

The straightforward extension of this fruitful approach to more general convex shapes was shown by us [13] to be impossible without fundamental alterations of the original approach. The main drawback came from the isotropy of the underlying weight functions in the long-wavelength limit, which in turn led to the isotropy of the DCF in the same limit with the consequence of the inability of such a DCF to account for any orientational instability of the isotropic phase. This major flaw was corrected by accounting for the correct zero-density limit of the DCF, which is the Mayer function [13]. This point is crucial in the extension of the theory to two-dimensional systems. Indeed, while the Mayer function of hard spheres can be written as a combination of weight functions, this is not the case for the two-dimensional hard disk fluid [12]. Instead of introducing an approximate Mayer function that can be written as a combination of weights as in Ref. [12], we directly introduce the correct Mayer function. The resulting approximation (and a variant) is presented in detail in the present work.

The remainder of this paper is set up as follows. In Sec. II we present the semi-analytical DCF approximation and the resulting thermodynamics for the general case, as well as some details concerning our Monte Carlo simulations and integral equations methods. Our approach of the orientationally ordered phases is also discussed in this section. Section III contains our results for several anisotropic fluids and the comparisons of the thermodynamic and structural properties with those obtained from the simulations and integral equations. Finally, in Sec. IV we gather our conclusions and perspectives.

II. THEORY

A. The geometrical approximation for the DCF

The complete version of this theory for the case of anisotropic fluid mixtures in three dimensions was presented in a previous article [13]. We consider an *inhomogeneous* mixture of N component fluids. The starting point is to write the excess free energy density Φ as a functional of a set of inhomogeneous weighted densities $\rho^{(\alpha)}(1)$, which are function of both the position $\vec{r}$ and orientation $\mathbf{\Omega}$ of particle **1**. The resulting excess free energy can be written as (with $\beta=1/k_BT$, the inverse Boltzmann temperature)

$$\beta F_{ex}[\rho]=\int d1\,\mathbf{\Phi}[\{\rho^{(\alpha)}(1)\}]. \tag{1}$$

This set of inhomogeneous weighted densities implies an exact knowledge of the fundamental geometrical measures or weights functions $w_i^{(\alpha)}(1)$ for each particle **1** belonging to the species i:

$$\rho^{(\alpha)}(1)=\sum_i \int d2\,\rho_i(2)w_i^{(\alpha)}(12), \tag{2}$$

where the sum is carried over all species i and $\rho_i(1)$ is the number density of species i for the inhomogeneous system. The shorthand notation $w_i^{(\alpha)}(12)$ stands explicitly for $w_i^{(\alpha)}(\vec{r_1}-\vec{r_2},\mathbf{\Omega_1})$. The n-body DCF can be obtained formally by successive functional differentiations of Eq. (1). In particular, for the pair DCF one has

$$\begin{aligned} c_{ij}(1,2)&=-\frac{\partial^2\beta F^{ex}}{\partial\rho_i(1)\partial\rho_j(2)}\\ &=-\sum_{\alpha,\beta}\int d3\,\Phi_{\alpha\beta}(3)w_i^{(\alpha)}(13)w_j^{(\beta)}(23), \end{aligned} \tag{3}$$

where we have used the same shorthand notation for the weights as in Eq. (2). The notation $\Phi_{\alpha\beta}(3)$ indicates the functional second derivative $\Phi_{\alpha\beta}(3)=\partial^2\Phi/\partial\rho^{(\alpha)}(3)\partial\rho^{(\beta)}(3)$.

In order to go further, the choice for Φ and for the weight functions must be specified. We will adopt here the two-dimensional (2D) scaled-particle theory (SPT) form [12], which is given by the following expression, written here for inhomogeneous systems:

$$\Phi[\{\rho^{(\alpha)}(1)\}]=-\rho_0(1)\ln[1-\rho_2(1)]+\frac{\rho_1^2(1)}{4\pi[1-\rho_2(1)]}. \tag{4}$$

In the case of *homogeneous* fluids, the weighted densities $\rho^{(\alpha)}$ are independent of the spatial variable **1** and simply reduce to the standard SPT variables ξ_α,

$$\rho^{(\alpha)}=\xi_\alpha=\sum_i \rho_i R_i^{(\alpha)}, \tag{5}$$

which are linked to the fundamental geometrical properties of the individual particle for each species i, which are the surface $R_i^{(2)}=S$, the perimeter $R_i^{(1)}=\ell$, and finally $R_i^{(0)}=1$.

From now on we consider only homogeneous systems, which are our main concern here. Using Eqs. (3)–(5) one can express the homogeneous pair DCF as

$$c_{ij}(1,2)=-\chi_S\Delta S_{ij}(1,2)-\chi_L\Delta L_{ij}(1,2)+\chi_0 F(1,2), \tag{6}$$

where we have explicitly

$$\begin{aligned} \chi_S&=\Phi_{22}=\frac{\xi_0}{(1-\xi_2)^2}+\frac{\xi_1^2}{2\pi(1-\xi_2)^3},\\ \chi_L&=\Phi_{21}=\frac{\xi_1}{2\pi(1-\xi_2)^2},\\ \chi_0&=\Phi_{20}=\frac{1}{(1-\xi_2)} \end{aligned} \tag{7}$$

and

$$\begin{aligned} \Delta S_{ij}(1,2)&=w_i^{(2)}(1)*w_j^{(2)}(2),\\ \Delta L_{ij}(1,2)&=w_i^{(2)}(1)*w_j^{(1)}(2)+w_i^{(1)}(1)*w_j^{(2)}(2),\\ F_{ij}(1,2)&=w_i^{(2)}(1)*w_j^{(0)}(2)+w_i^{(0)}(1)*w_j^{(2)}(2)\\ &\quad+\frac{1}{2\pi}w_i^{(1)}(1)*w_j^{(1)}(2), \end{aligned} \tag{8}$$

where the asterisk denotes convolution. The most remarkable feature of Eq. (6) is the nice decoupling between density-dependent coefficients χ_α and spatial variables through the geometrical functions S_{ij}, Lij, and F_{ij}.

We turn now to the determination of the weight functions and their general properties. The prescription of the one-body function $\rho_i(1)$ contains the information about the symmetry of the phase under study. The weights, on the other hand, by construction, should contain information only about the geometry of the particle. Then Eq. (2) tells us that the weighted densities $\rho_\alpha(1)$ will carry the same information as $\rho_i(1)$ about the symmetry of the phase that is studied. Once this point is clarified, one can write down the formal expansion of the weights in a basis of rotational invariants. In two dimensions, with the choice of variables $\vec{r}=(r,\theta_r)$ and $\mathbf{\Omega}=(\theta)$, such an expansion reads (with all the angles chosen in a laboratory fixed frame)

$$w_i^{(\alpha)}(\vec{r},\mathbf{\Omega})=\sum_m w_{i;m}^{(\alpha)}(r)e^{im(\theta_r-\theta)}. \tag{9}$$

The Fourier-Bessel transform of the weight is [5]

$$\tilde{w}_i^{(\alpha)}(\vec{k},\mathbf{\Omega})=\sum_m \tilde{w}_{i;m}^{(\alpha)}(k)e^{im(\theta_k-\theta)}, \tag{10}$$

with the expression for the transform of the expansion coefficients

$$\tilde{w}_{i;m}^{(\alpha)}(k)=i^m\int d\vec{r}\; w_{i;m}^{(\alpha)}(r)J_m(kr). \tag{11}$$

From the properties of the Bessel function $J_m(x)$ in the limit $x\to 0$ one gets by using Eqs. (2) and (5)

$$\tilde{w}_{i;m}^{(\alpha)}(k=0)=\delta_{m0}R^{(\alpha)}. \tag{12}$$

Equation (12), which is very general and independent of the symmetry of the phase in consideration, implies two important points. First, the weights are *isotropic* in the limit $k\to 0$. This is the same point that was raised in the 3D case [13]. Taking the Fourier-Bessel transform of Eq. (6), one sees that the convolution products become products and the above conclusion leads to the isotropy of the DCF in the same limit $k\to 0$. This is clearly an unphysical behavior, as the DCF must account for the orientational instability of the isotropic phase [14]. This isotropy is common to all order DCF's that can be derived within this formalism. It is important to note that this flaw of the theory depends only on the fact that we have introduced the weighted densities through Eq. (2). In view of the present result, it seems that the previous success of the theory is applicable only for fluids of spherical particles.

Before we see how this flaw can be corrected, let us get to the second point, which is in fact a hint to how we can write down explicit expressions for the weights. Indeed, Eq. (12) shows that the weights are linked to the SPT geometrical variables $R^{(\alpha)}$ in Eq. (5). It is then tempting to attribute the same geometrical meaning to the corresponding weights. Following then our study of the 3D case, we define the volume weight as

$$w_i^{(2)}(\vec{r},\mathbf{\Omega})=\frac{1}{2\pi}H(|\vec{r}-\vec{R}_i(\mathbf{\Omega})|)$$

and the surface weight as

$$w_i^{(1)}(\vec{r},\mathbf{\Omega})=\frac{1}{2\pi}\sqrt{1+\frac{1}{r^2}\left(\frac{dr}{d\theta}\right)^2}\,\delta(R_i(\mathbf{\Omega})-r). \tag{13}$$

In these equations $\vec{R}_i(\mathbf{\Omega})$ is a vector pointing to the external perimeter of the particle of species i, which is oriented by $\mathbf{\Omega}$ in the laboratory fixed frame. These two definitions have the advantage of satisfying Eq. (5), although they are not the unique possible representations that can lead to this result. However, they reduce the corresponding weights for hard disks.

From these definitions we see that the entire weight function formalism is restricted to two-dimensional *convex* shapes [it is naturally imposed by the unity of the vector $\vec{R}_i(\mathbf{\Omega})$ for each orientation $\mathbf{\Omega}$, which is not true for nonconvex shapes]. The extension to nonconvex shapes is not outruled, however, and the generalization of the present formalism to tangent disks, for example, can be formulated in very much the same way as for the tangent sphere case in three dimensions [15].

Using these definitions, we see that the terms in Eqs. (8) gather a different geometrical significance. $\Delta S_{ij}(1,2)$ is now the surface of the geometrical overlap between particles 1 and 2 belonging, respectively, to species i and j. Similarly, $\Delta L_{ij}(1,2)$ is the perimeter of this overlap area.

As concerns the third weight $w^{(0)}$, although one could construct a distribution that satisfies the correct $k=0$ limit [16], we can see that there is no need to do so. Indeed, in the limit of zero density, the pair DCF must reduce to the Mayer function $f_{M;ij}(12)=\exp[-\phi_{ij}(1,2)/k_BT]-1$, where $\phi_{ij}(1,2)$ is the hard core interaction between particles 1 and 2 of, respectively, species i and j. From Eq. (7) we see that in the zero-density limit we have $\chi_V=\chi_L=0$ and $\chi_0=1$. Therefore, our approximation leads to $c_{ij}(1,2)|_{\rho=0}=F_{ij}(1,2)$. Clearly, $F_{ij}(1,2)$, as defined in Eq. (8), is an *isotropic* function in the limit $k=0$ because it is expressed as a product of weight functions. As a consequence, it cannot be equal to $f_M(1,2)$, which is fundamentally anisotropic in this limit. Therefore, our approximation for the DCF in two dimensions is to replace in Eq. (6) F_{ij} by the Mayer function $f_{M;ij}(1,2)$.

In particular, for the one-component system this approximation reads

$$c(1,2)=-\chi_S\Delta S(1,2)-\chi_L\Delta L(1,2)+\chi_0 f_M(1,2). \tag{14}$$

For the isotropic phase, the rotational invariant expansion of the DCF can be conveniently written in intermolecular frame as [5]

$$c(1,2)=\sum_{m,n} c^{mn}(r_{12})\psi^{mn}(\theta_{1r},\theta_{2r}), \tag{15}$$

where $\theta_{ir}=\theta_i-\theta_r$ and $\psi^{mn}(\theta_1,\theta_2)=\exp[i(m\theta_1+n\theta_2)]$ is the rotational invariant of the isotropic phase [5] (all the angles being measured in the laboratory fixed frame). The Fourier-Bessel transform of the DCF is expanded as

$$\tilde{c}(1,2)=\sum_{m,n}\tilde{c}^{mn}(k)\psi^{mn}(\theta_{1k},\theta_{2k}), \tag{16}$$

with the angles now measured in the k frame. The expansion coefficients are given by [5]

$$\tilde{c}^{mn}(k)=i^{m+n}\int d\vec{r}\; c^{mn}(r)J_{m+n}(kr). \tag{17}$$

The Mayer function and the geometrical functions ΔS and ΔL can also be expanded similarly. The expansion coefficients of the latter functions can be derived from Eq. (8),

$$\tilde{\Delta}S^{mn}(k)=\tilde{w}_m^{(2)}(k)\tilde{w}_n^{(2)}(k), \tag{18}$$

$$\tilde{\Delta}L^{mn}(k)=\tilde{w}_m^{(2)}(k)\tilde{w}_n^{(1)}(k)+\tilde{w}_m^{(1)}(k)\tilde{w}_n^{(2)}(k).$$

This completes the prescription of the geometrical approximation for the DCF.

B. A second approximation for the DCF

There is an alternate possibility, similar to the third DCF approximation in three dimensions [13]. In such a model, one could assume the form of the DCF similar to Eqs. (6) or (14) and compute the χ_α coefficients from the virial and compressibility equations of state. We have shown in Ref. [13] that this approach gives the Percus-Yevick (PY) solution for hard spheres when the appropriate equations of state are used. The method is also applicable here and is detailed below. The last coefficient χ_0 can be determined from the virial equation [5]

$$Z_v=\frac{\beta P_v}{\rho}=1+\frac{\rho}{4\pi}\int\int d\mathbf{u}_1 d\mathbf{u}_2[\sigma(12)]^2 g[\sigma(12)], \tag{19}$$

where $\sigma(12)$ is the contact distance between two molecules with orientations $\mathbf{u}_1$ and $\mathbf{u}_2$. Assuming that the pair distribution function $g(12)$ is zero inside the hard core (which is true for the PY approximation, for example), one gets easily χ_0 as

$$\chi_0=\frac{Z_v-1}{\rho B_2}, \tag{20}$$

where the second virial coefficient B_2 can be written as $B_2=(1/4\pi)\int\int d\mathbf{u}_1 d\mathbf{u}_2[\sigma(12)]^2$. The first two coefficients χ_S and χ_L can be derived from two coupled equations. The equation relating the compressibility (which uses the compressibility pressure βP_c) to the DCF [see Eq. (23)] gives directly

$$\chi_S S+2\chi_L\not{\ell}=\frac{(\partial/\partial\rho)\beta P_c+2Z_v-1}{\rho S}. \tag{21}$$

The second equation can be derived from the Ornstein-Zernike (OZ) equation written for zero separation and identical orientations of the two particles. Again, by assuming that $g(12)=0$ inside the hard core one gets

$$\chi_S S+\chi_L\not{\ell}=-\frac{\partial(\beta P_c)}{\partial\rho}+\chi_0. \tag{22}$$

These two equations can be trivially solved for χ_S and χ_L, providing thus the second approximation for the DCF solely in terms of Z_c and Z_v. In the present case and in the absence of known analytical expressions for the virial and compressibility equations of state, one could use here the SPT EOS derived from Eq. (4) as a single input. This is precisely the method we have adopted in the numerical applications.

There is very little numerical difference between the two approximations proposed here. They both yield the SPT compressibility by construction (see Sec. II C). In Sec. III we show that the first approximation is somewhat superior, in the sense that it yields orientational instabilities in better agreement with the hypernetted chain (HNC) and simulation results. The main drawback of the second approximation is that it is not straightforward to extend it to mixtures. We also note that none of these approximations guarantees that the corresponding pair distribution function $g(12)$ determined through the OZ equation will be zero inside the hard core (except of course in the zero-density limit). It is not obvious how this stringent constraint can be incorporated in either of our approximations.

We now turn to the calculation of properties such as the equation of state, the instability criteria for the isotropic phase, and finally our approach of the nematic phase.

C. Thermodynamic properties

From the DCF one can compute directly the compressibility of the isotropic phase through the relation

$$\left(\frac{\partial\beta P}{\partial\rho}\right)_T=1-\rho\tilde{C}^{00}(k=0). \tag{23}$$

It is interesting to know if the geometrical approximation gives a compressibility that is consistent with the SPT free energy. The answer is yes because the second virial coefficient, which is correctly given by the geometrical approximation, that is, $B_2=S+L^2/2\pi$, is also given by the original DCF because of the relations $-2B_2=\tilde{f}_M^{00}(k=0)=\tilde{F}^{00}(k=0)$, the last one following from Eqs. (18) and (12). The resulting equation of state is then

$$\beta P=\frac{\xi_0}{1-\xi_2}+\frac{1}{4\pi}\frac{\xi_1^2}{(1-\xi_2)^2}. \tag{24}$$

Similarly, the chemical potential is given by

$$\beta\mu=\ln\left(\frac{\xi_0}{1-\xi_2}\right)+\frac{\xi_2}{1-\xi_2}+\frac{1}{2\pi}\frac{\xi_1^2}{\xi_0(1-\xi_2)}+\frac{1}{4\pi}\frac{\xi_1^2\xi_2}{\xi_0(1-\xi_2)^2}. \tag{25}$$

The explicit expression for the pressure allows us to calculate all the virial coefficients in a single formula

$$B_n = S^{n-1} + \frac{n-1}{4\pi} L^2 S^{n-2}, \tag{26}$$

which is of course exact only for B_2.

The orientational stability of the isotropic phase can be derived from the convexity of the free energy [14] and is described by the positivity of the different modes Δ_m given by [5]

$$\Delta_m = 1 - \rho \tilde{c}^{m-m}(k=0) = \frac{1}{1+\rho \tilde{h}^{m-m}(k=0)} > 0. \tag{27}$$

For the present model the Δ_m are simply given by

$$\Delta_m = 1 - \rho \chi_0 \tilde{F}_M^{m-m}(k=0), \tag{28}$$

where χ_0 can be evaluated from Eq. (7) in the case of the first approximation or by Eq. (20) for the second approximation. Usually, the isotropic-nematic transition follows the destabilization of the mode Δ_2, which is the two-dimensional analog of the inverse Kerr constant and is known to diverge at the limit of the orientational stability of the isotropic phase. The divergence of Δ_4^{-1} can occur in some cases and in three dimensions this is linked to the appearance of a *cubatic* order [17,18], which is characterized by short stack pilings of about four particles, which themselves tend to stay perpendicular to each other. The existence of a two-dimensional analog of this type of order is an open question.

D. Orientational order

The one-body density $\rho(1)$ contains the description of the orientational order. In the case of positionally homogeneous fluid this function will depend only on the relative orientation with respect to the global director $\vec{n}$, that is, $\rho(1) = \rho(\theta)$, where $\cos(\theta) = \vec{n} \cdot \vec{u}$, with $\vec{u}$ describing the orientation of the molecule. From Eq. (2) we see that the weighted densities ρ_α should have the same angular dependence. However, a closer look reveals that the isotropy of the weight functions leads to weighted densities that are independent of the orientation of the molecule and Eq. (5) is again recovered. Hence this formalism leads to an identity of the nematic and isotropic phases.

If we wish to use the corrected approximation for the DCF, the weighted density formalism must be abandoned and the one-body function must be computed by other methods. There is an exact equation that links the one-body function to the DCF of the corresponding *inhomogeneous* phase [9]

$$\partial_1 \ln[\rho(1)] = \int d2\, c(1,2) \partial_2 \rho(2). \tag{29}$$

From this point two pathways are possible. Either we try to propose an approximate DCF of the nematic phase or we use the DCF of the isotropic phase in the equation above in order to compute $\rho(1)$. In principle, the DCF of the nematic phase should reflect the symmetry and the invariance properties of the phase under study. Here the geometrical DCF brings up here an important issue. Indeed, if the major contributions to the DCF come from properties such as the two-particle overlap geometry or the Mayer function, which are independent of symmetries lower than that of the isotropic phase, this strongly suggests that a good approximation of the DCF may also have the same property. If we replace the DCF in Eq. (29) by the geometric approximation, the resulting equation can be solved [18], with the result for $\rho(\theta) = \rho f(\theta)$

$$f(\theta) = \frac{\exp[\rho W(\theta)]}{Z}, \tag{30}$$

where

$$W(\theta) = \frac{1}{2\pi} \int_0^{2\pi} d\theta' f(\theta') \tilde{c}(k=0, \theta - \theta'), \tag{31}$$

with the normalization factor $Z = \int d\theta \exp[\rho W(\theta)]$. The thermodynamic properties can now be derived from the free energy of the ordered phase whose excess part can be obtained by the functional integration of the DCF [19] as

$$\phi = \beta F_{ex}[\rho]/V = -\int \int d1\, d2\, \rho(1)\rho(2) \int_0^\lambda d\lambda\; c(1,2;\lambda\rho). \tag{32}$$

The ideal part of the free energy is given by $\beta F_{id}[\rho]/V = \int d1\, \rho(1)\{\ln[\rho(1)] - 1\}$. The resulting chemical potential and pressure can be derived from the standard thermodynamic relations $\beta\mu = \partial(\beta F/V)/\partial\rho$ and $\beta P = \rho \partial(\beta F/V)/\partial\rho - \beta F/V$.

E. Integral equation approaches and computer simulations

We have also solved the PY and HNC integral equations using the techniques developed in Ref. [5] for various molecular shapes. These techniques allows to obtain the pair DCF and the pair correlation function $g(1,2)$ from the sole input of the pair interaction, which is in fact the Mayer function $f_M(1,2)$ for hard bodies. From previous work [5] it was found that these techniques allow us to obtain an accurate pair correlation function, hence the DCF, for moderately high densities and aspect ratios. In fact, it was found that the two approximations often bracket the thermodynamic and structural results obtained from the simulations. These techniques can thus serve as a test of the geometrical approach. In particular, it is interesting to check if the geometrical DCF is PY-like in all aspects.

Finally, we have also used Monte Carlo (MC) simulation methods to get the pressures (*NPT* ensemble simulations) and some of the pair correlation function projections $g^{mn}(r)$ (in the *NVT* ensemble), mainly those corresponding to indices $(m,n) = (0,0)$, $(2,-2)$, $(4,-4)$, and some others. The projections $(m,-m)$ in particular reflect the growth of orientational correlations in the vicinity of densities for which ordered phases can appear. The DCF cannot be measured directly by simulations. One needs to invert the total pair correlation function by using the Fourier-Bessel transform of the Ornstein-Zernike equation [20]. This means that one must compute all the projections $g^{mn}(r)$ needed for a given maximum value of m. Although this method is quite feasible for moderate densities (about 20% of the close packing) when the pair correlation function is not long ranged and decays within the simulation box length, this is not the case

at higher densities when the density correlations range can exceed substantially the box length. If this is the case, the Fourier-Bessel transforms of the pair correlations cannot be handled satisfyingly, as the small k values are inaccurate. In order to avoid these complications, we have simply compared the pair correlations obtained from the geometrical DCF to those obtained in the simulations. Surprisingly, despite the fact that these pair correlations are nonzero inside the hard core region, the overall agreement was found to be quite good. The detailed comparisons are discussed in the next section for several model fluids.

III. RESULTS FOR 2D FLUIDS

In this section we consider our results for various two-dimensional convex particles fluids such as the hard ellipse, diskorectangle, cut disk, and finally hard needle fluids. The unit length is taken to be that of the underlying hard disk diameter σ (for the hard needle case it is the needle length). The various molecular parameters are the aspect ratio κ, the rectangle length $L^*=L/\sigma$, and the cut disk thickness $d^*=d/\sigma$. The reduced density is defined as $\rho^*=\rho\sigma^2$ and the packing fraction is $\eta=\rho S$, where S is the particle surface.

One of the ingredients common to both the geometrical DCF and the integral equation methods is the Mayer function, whose projections $f_M^{mn}(r)$ must be calculated numerically. For the molecular interaction symmetry considered here, only even values of m and n are retained [5]. Expansion terms up to $n,m<6$ were retained, as in the previous work [5], where it was found that this choice was sufficient to ensure that the numerical solutions of the integral equation were not affected by the truncation of the rotational invariant expansion. The numerical calculation of the $f_M^{mn}(r)$ has been outlined in Refs. [5] and [16].

NPT and *NVT* ensemble Monte Carlo simulations were conducted for both the diskorectangle and cut disk fluids: diskorectangles of rectangle lengths $L^*=1, 2$, and 5 and cut disks of thicknesses ranging from $d^*=0.1$ to 0.5. The number N of molecules in the central box was around 200 (the exact number varies with the shapes and the aspect ratio, according to the maximum packing possibility). In all cases, equilibration runs were about 10 000–20 000 steps and the productions were run from 50 000–200 000 steps in some cases. Long runs were needed, for example, in the case of very elongated shapes, mainly to determine if the fluid was nematically ordered. Indeed, in such cases, it was found that the nematic order of the fluid was lost very slowly in the course of the runs. No detailed study of the size dependence on the order parameter was done here, however, nor were the phase transitions located. The aim of the present work was only to provide the pressures and the pair correlations in the *isotropic* phase. In some cases, nematic phases were explored and particularly the 2D analog of the cubic phase for the cut disks was also tracked to some extent, which is discussed below.

Figure 1 shows a comparison between the density-dependent coefficients χ_α of the two approximations introduced in Sec. II for a fluid of ellipses of aspect ratio $\kappa=4$. One can see that the surface term dominates totally the line (perimeter) and Mayer terms at high densities. Also, the surface terms χ_S from both approximations are closer to each other. The direct consequence is that the corresponding DCFs are quite similar in the high-density regime. On the contrary, the two other terms χ_L and χ_0 tend to have divergent behavior at high densities. In particular, the Mayer coefficient χ_0 for the second approximation becomes much larger in this regime. Consequently, from Eq. (28) one sees that the second approximation will predict an orientational instability at a density lower than that of the first approximation. This last point is in disfavor of the second approximation, as the first one already tends to predict orientational instability densities lower than those predicted by computer simulations (see Fig. 5 and the discussion below).

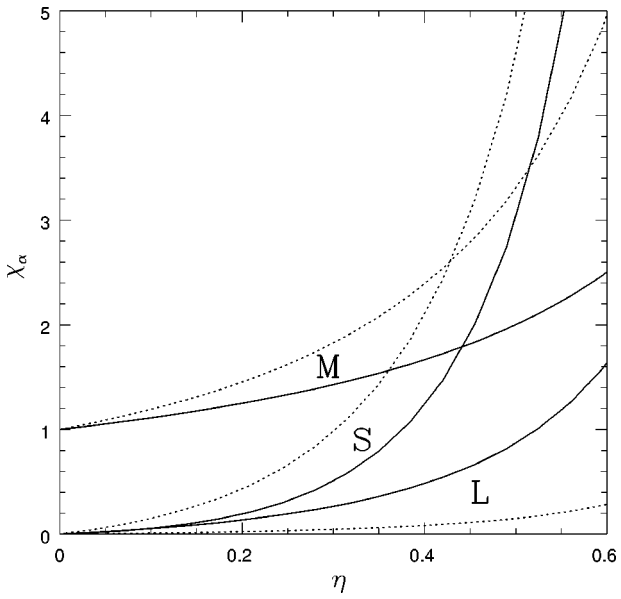

FIG. 1. Density-dependent coefficients for the pair DCF, for the two models discussed in the text, in the case of the hard ellipse fluid for the aspect ratio $\kappa=4$. The solid lines and the dotted line are, respectively, for the first and second approximations. The letters help identify the coefficients corresponding to the surface (S), line (or perimeter) (L), and the Mayer function (M) terms.

A. Pressure

The pressures for fluids of the ellipses of aspect ratio $\kappa=2$, 4, and 6 calculated from Eq. (24) are shown in Fig. 2(a), together with the MC results of Cuesta and Frenkel [2]. The hard disk results ($\kappa=1$) are also shown. The nematic branches are shown as filled circles. One sees that the agreement is quite good at small to medium densities for all elongation and deteriorates for high densities and large elongation. At high densities the theoretical pressures are always above that of the numerical ones. This feature must be linked to the fact that the higher-order virial coefficients are smaller than those obtained from Eq. (26). In particular, it was shown that for large aspect ratios (the hard needle case, for example), some of the higher-order virial coefficients could become negative [2]. This is in contrast to Eq. (26), which predicts strictly positive virial coefficients at all orders. The compressibility pressures from the PY and HNC integral equations are also shown for the isotropic phase. The pressures for diskorectangles are given in Fig. 2(b) and for cut disks in Fig. 2(c). Our Monte Carlo results for the pressures

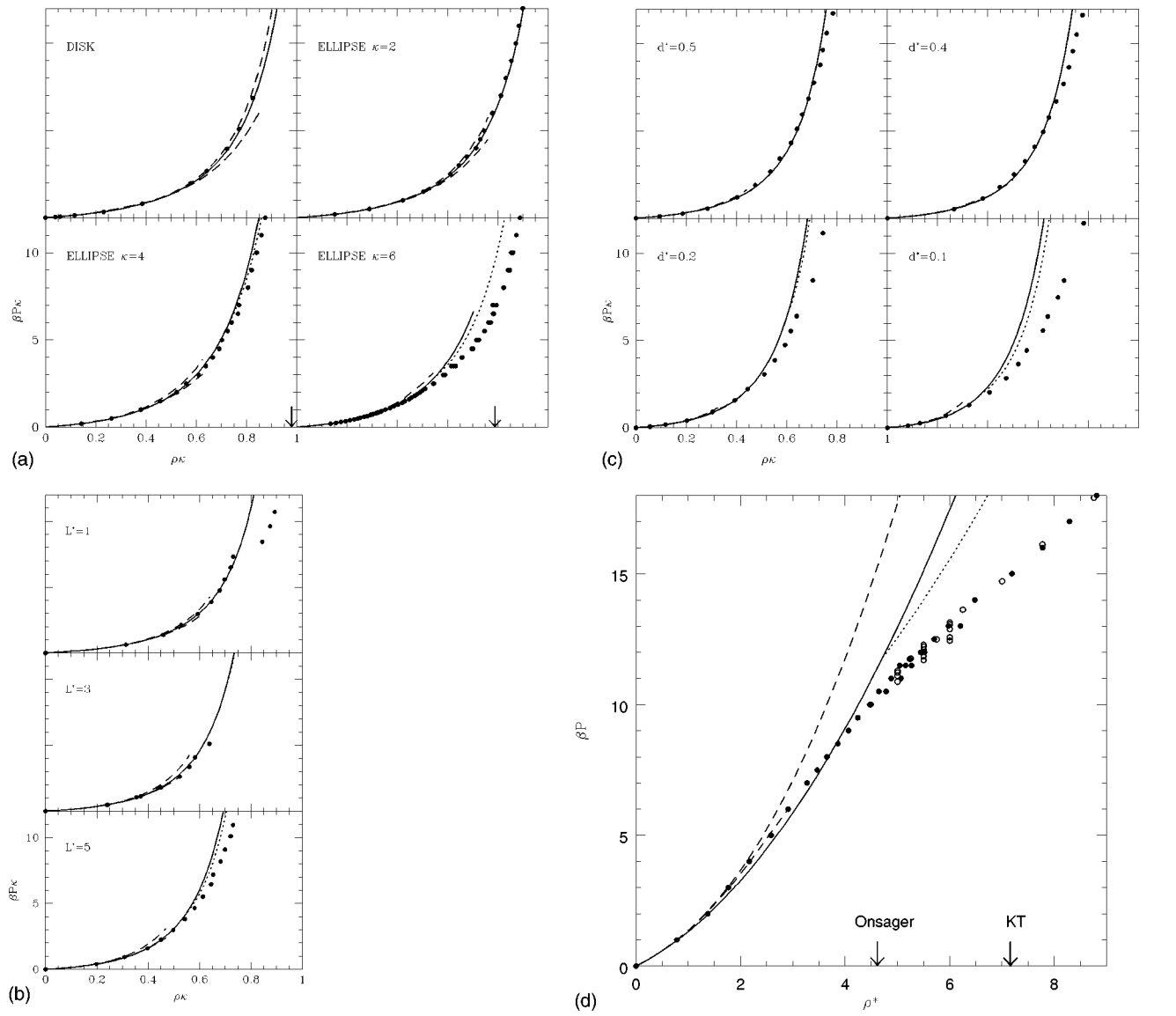

FIG. 2. (a) Equation of state $(\beta P/\rho)\kappa$ versus the density $\rho\kappa$ for the hard ellipse fluid and for aspect ratios $\kappa=1,\ 2,\ 4$, and 6. The solid line is for the first approximation in the isotropic phase [Eq. (20)] and the dotted line is for the corresponding nematic phase. The dashed lines are compressibility route pressures from the PY (upper curve) and HNC (lower curve) approximations. The filled circles are simulation results from Ref. [2]. (b) Equation of state for the hard diskorectangle fluid and for rectangle length $L^*=1,\ 3$, and 5 ($\kappa=L^*+1$). The symbols are the same as in (a). (c) Equation of state for the hard cut disk fluid and for thicknesses $d^*=0.5,\ 0.4,\ 0.2$, and 0.1 ($\kappa=1/d^*$). The symbols are the same as in (a). (d) Equation of state for the hard needle fluid. The symbols are the same as in (a). The dots and squares are from Ref. [21] (filled circles for the isotropic phase and open circles for the nematic phase). The Onsager and KT transitions are shown by arrows.

are given in Tables I and II. The general features are comparable to those of Fig. 2(a). It seems that the SPT geometrical results become worse as the aspect ratio increases. We see that, on the contrary, the HNC compressibility results become in closer agreement with the simulation results, whereas the PY results are always too high. We note that for both these theories, the density range for the isotropic phase decreases strongly with the increase of the aspect ratio.

These two tendencies are more striking when examining the hard needle case in Fig. 2(d). In this case the SPT geometrical variables are $S=0$ and $\mathcal{L}=2$. The second virial coefficient is exact again ($B_2=1/2\pi$), but all higher-order coefficients are zero. As a consequence, the geometrical model is reduced exactly to the Onsager model, with $c(1,2)=f_M(1,2)$. Hence the SPT EOS is lower that the MC results [21] at medium densities. In particular, we observe that the isotropic-nematic transition predicted by our approach is identical to the Onsager prediction at $\rho^*=4.71$. As concerns the integral equations results, we see that the HNC compressibility route gives nearly perfect results, whereas the PY theory gives pressures that are too high. One must note also the very small density range over which the two theories can be solved. This range is particularly small for the HNC theory (smaller than the Onsager transition density), whereas for the PY theory the density range extends up to values larger than $\rho^*=10$, which are larger than the Kosterlitz-Thouless (KT) transition density. This behavior has some similarities to the solution of the two integral equa-

TABLE I. Compressibility factor $Z=\beta P/\rho$ versus density $\rho^*=\rho\sigma^2$ for the diskorectangle fluids obtained by Monte Carlo simulations.

$L^*=1$		$L^*=3$		$L^*=5$	
Z	ρ^*	Z	ρ^*	Z	ρ^*
2.0	0.1569	2.0	0.0600	2.0	0.0331
3.0	0.2297	3.0	0.0927	3.0	0.0512
4.0	0.2636	4.0	0.1125	4.0	0.0663
5.0	0.2967	5.0	0.1306	5.0	0.0750
6.0	0.3227	6.0	0.1401	6.0	0.0829
7.0	0.3391	7.0	0.1456	7.0	0.0905
8.0	0.3486	8.0	0.1596	8.0	0.0968
9.0	0.3605	9.0	0.1971	9.0	0.1021
10.0	0.3655	10.0	0.2009	10.0	0.1075

tions for the 3D fluid of hard platelets [22]. We return to this point in the discussion of the instability of the isotropic phase.

The nematic branches for the hard ellipse fluid of aspect ratios 4 and 6 in Fig. 2(a) indicate clearly that the present theory predicts an isotropic-nematic phase transition at densities too low compared to simulation results. It is reasonable to think that the same trend is also true for the other convex bodies.

B. Structure

In this section we compare direct and pair correlation functions obtained from the present theory and the two integral equations. In the case of the pair correlations, comparisons with computer simulations are also shown.

Some expansion coefficients $c^{mn}(r)$ of the DCFs for the fluid of hard ellipses of aspect ratio $\kappa=4$ are shown in Fig. 3(a) for the density $\rho^*=\rho\sigma^2=0.15$, where σ is the breadth of the ellipse. The density is chosen to be close to the highest density for which either of the integral equation could be solved. This convention is also adopted for other bodies. One sees that for the isotropic component $c^{00}(r)$, the first geometrical approximation for the DCF interpolates quite nicely between the corresponding HNC and PY results. This behavior is no longer true for higher-order expansion coefficients of the DCF, although the agreement between the three different approaches is closer than that found for the isotropic component. Globally, from the inspection of the components displayed in Fig. 3(a), one sees that the HNC DCF is the most structured of all three, whereas the geometrical DCF is the less structured one. One also sees the PY nature of the geometrical approximation in the relatively close resemblance of features between these two DCFs. The agreement between these two approximations become better at lower densities. The same trends are observed for lower and higher aspect ratios, although the difference between the geometrical DCF and the two other approaches deteriorates with increasing aspect ratios.

TABLE II. Compressibility factor $Z=\beta P/\rho$ versus density $\rho^*=\rho\sigma^2$ for the cut disk fluids obtained by Monte Carlo simulations.

$d^*=0.1$		$d^*=0.2$		$d^*=0.4$		$d^*=0.5$	
Z	ρ^*	Z	ρ^*	Z	ρ^*	Z	ρ^*
1.5	0.8161	1.2	0.2773	2.0	0.6639	1.2	0.1872
2.0	1.2948	1.5	0.5873	3.0	0.9493	1.5	0.3711
3.0	2.3244	2.0	1.0145	4.0	1.1188	2.0	0.5679
4.0	3.2565	3.0	1.5213	5.0	1.2599	3.0	0.8039
5.0	4.0622	4.0	1.9627	6.0	1.3691	4.0	0.9475
6.0	4.7286	5.0	2.2210	7.0	1.4658	5.0	1.0697
7.0	5.2113	6.0	2.5547	8.0	1.5499	6.0	1.1430
8.0	5.5415	7.0	2.7611	9.0	1.6069	7.0	1.2339
9.0	6.1870	8.0	2.9655	10.0	1.6784	8.0	1.2818
10.0	6.3837	9.0	3.0786	11.0	1.7533	9.0	1.3230
11.0	6.7888	10.0	3.1989	12.0	1.8053	10.0	1.3722
12.0	7.0356	12.0	3.5186	13.0	1.8439	11.0	1.4148

Figure 3(b) shows the DCF for the fluid of hard diskorectangles of aspect ratio $\kappa=4$ ($L^*=3$) at density $\rho^*=0.12$. One sees that the major trends seen here are similar to those observed for the hard ellipse DCF. One can note that the isotropic component of the geometrical DCF is now closer to that of the HNC theory. The density and aspect ratio dependences are quite similar to that of the ellipse fluid.

Figure 3(c) shows the three DCFs for the fluid of hard cut disks of aspect ratio $\kappa=5$ (thickness $d^*=0.2$) at density $\rho^*=1.5$. Now the differences between the geometrical approach and the two others are more marked. First the isotropic component is no longer an interpolation between the HNC and PY results. Then the $c^{02}(r)$ is not in such good agreement with the others. We note that, similarly to the hard ellipse and diskorectangle fluid cases, the differences are less marked at lower densities. They also tend to disappear at smaller aspect ratios, albeit larger thickness, which makes the shape closer to the hard disk. There are two reasons for the differences seen in Fig. 3(c). First, the cut disk shape is a two-dimensional oblate shape (the particle axis is perpendicular to the longer symmetry axis) and our investigation of oblate shapes in three dimensions [13] has shown that the geometrical approach was not very good in this case. In fact, there are some resemblances between the behavior of the DCF components c^{00} and c^{02} in two dimensions and the corresponding ones in c^{000} and c^{202} in three dimensions. The second point concerns the fact that cut disks of thickness $d^*=0.2$ have a tendency to exhibit a two-dimensional cubatic phase as will be shown subsequently, whereas the geometrical approach predicts an instability towards a nematic phase. This reflects the density couplings that builds up into the PY and mainly the HNC DCFs and cannot be represented simply as a linear function of the Mayer function as in Eq. (14). We return to this point in the discussion of the orientational instability of the isotropic phase. A similar conclusion was also reached in Ref. [18] in the study of the cut sphere fluids.

The pair correlations for the three types of fluids encountered above are displayed in Figs. 4(a)–4(c) together with computer simulations results. For the hard ellipse fluid only the components $g^{m-m}(r)$ for $m=0, 2,$ and 4 are available from computer simulations [2,5]. These projections are compared with the three theoretical results for the fluid of hard ellipse of $\kappa=4$ at density $\rho^*=0.152$ in Fig. 4(a). As mentioned at the end of Sec. II B, the pair correlation function

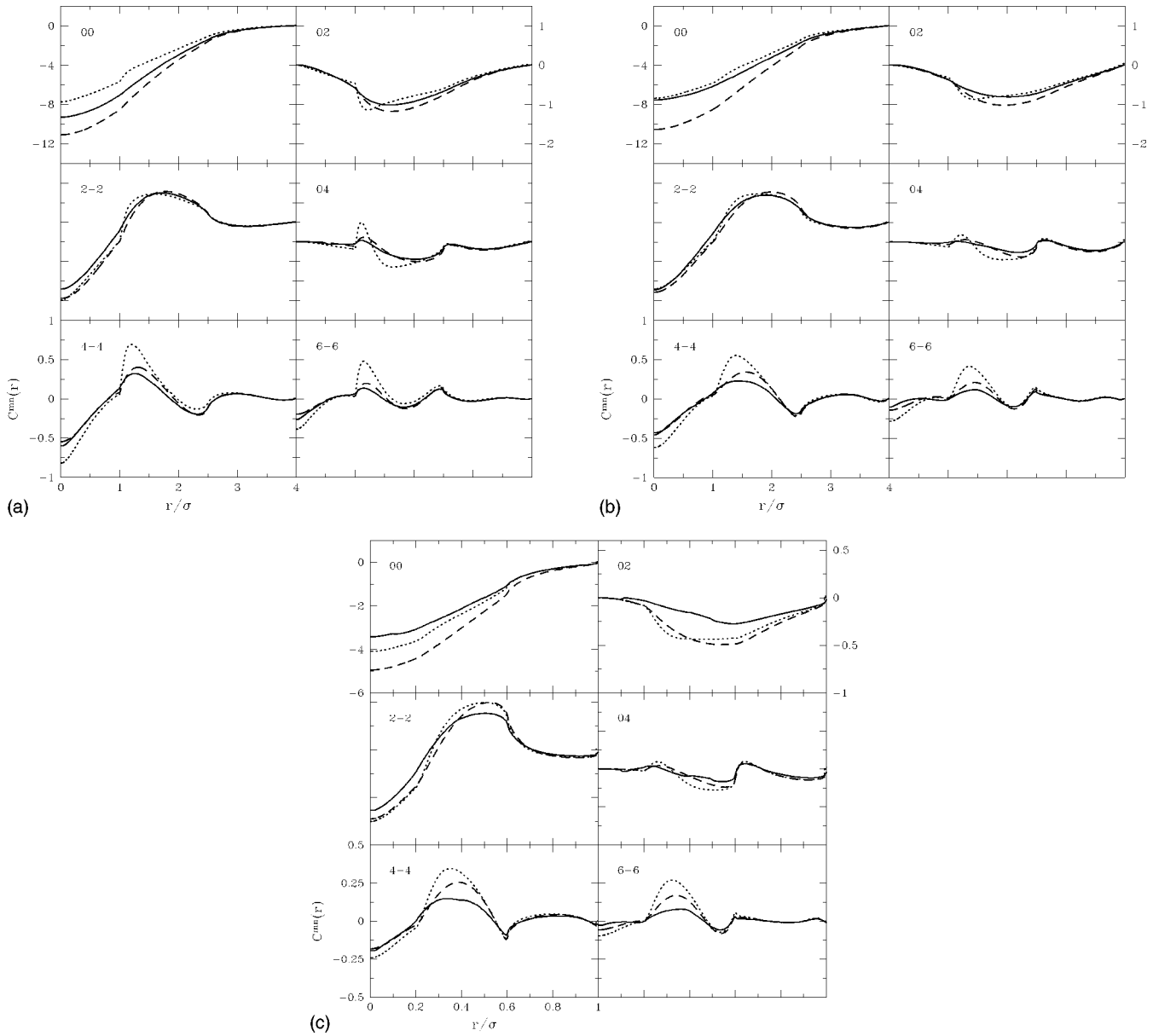

FIG. 3. (a) Expansion coefficients $c^{mn}(r)$ of the pair DFC for the hard ellipse fluid of aspect ratio $\kappa=4$ at the density $\rho^*=0.15$. The solid line is for the first approximation, the dotted line for the HNC theory, and the dashed line for the PY theory. The projection indices (m,n) are indicated on the corresponding panels. The vertical labeling for the projections (0,2) and $(2,-2)$ is the same, and similarly for projections (0,4), $(4,-4)$, and $(6,-6)$. (b) Expansion coefficients $c^{mn}(r)$ of the pair DFC for the hard diskorectangle fluid for $L^*=3$ at the density $\rho^*=0.12$. The lines and labeling conventions are the same as in (a). (c) Expansion coefficients $c^{mn}(r)$ of the pair DFC for the hard cut disk fluid for $d^*=0.2$ at the density $\rho^*=1.5$. The lines and labeling conventions are the same as in (a).

$g(1,2)$ corresponding to the geometrical DCF will not be zero for overlapping configurations of particles 1 and 2. This flaw of the geometrical model was also mentioned in the 3D case [13]. This feature of the pair correlation function can be clearly seen in Figs. 4(a)–4(c), at least in the $r/\sigma \leqslant 1$ region. However, it is surprisingly PY-like in other regions, mainly for the isotropic component $g^{00}(r)$. The fact that this theory is able to reproduce the isotropic nematic instability can be seen in the long-range correlations growth of the $g^{2-2}(r)$ component, in accord with the computer simulation and HNC results, but at variance with the PY results. In addition, one notes the oversized first peak, very much HNC-like, which again experiences the strong short-range alignment.

Figure 4(b) shows more components of the pair correlation for the fluid of hard diskorectangles for $\kappa=6$ and at density $\rho^*=0.078$. Globally, features similar to that observed above for the hard ellipse case. We note that the HNC results tend to exaggerate the first peak, which shows the nearest-neighbors alignment tendency, whereas the PY results totally miss this feature. The PY theory is in better agreement in the range where particles have a loose perpendicular alignment, as seen in g^{4-4} around $r^*=3$. It seems that the HNC theory overemphasizes the ordering tendencies, whereas the PY theory misses the same tendencies. The geometrical approach indicates a global ordering from the g^{2-2} component. These results are corroborated by the orientational instability analysis.

The case of the hard cut disk fluid is displayed in Fig. 4(c) for the thickness $d^*=0.2$ and density $\rho^*=1.5$, which is not really a high density. This choice was dictated by the fact

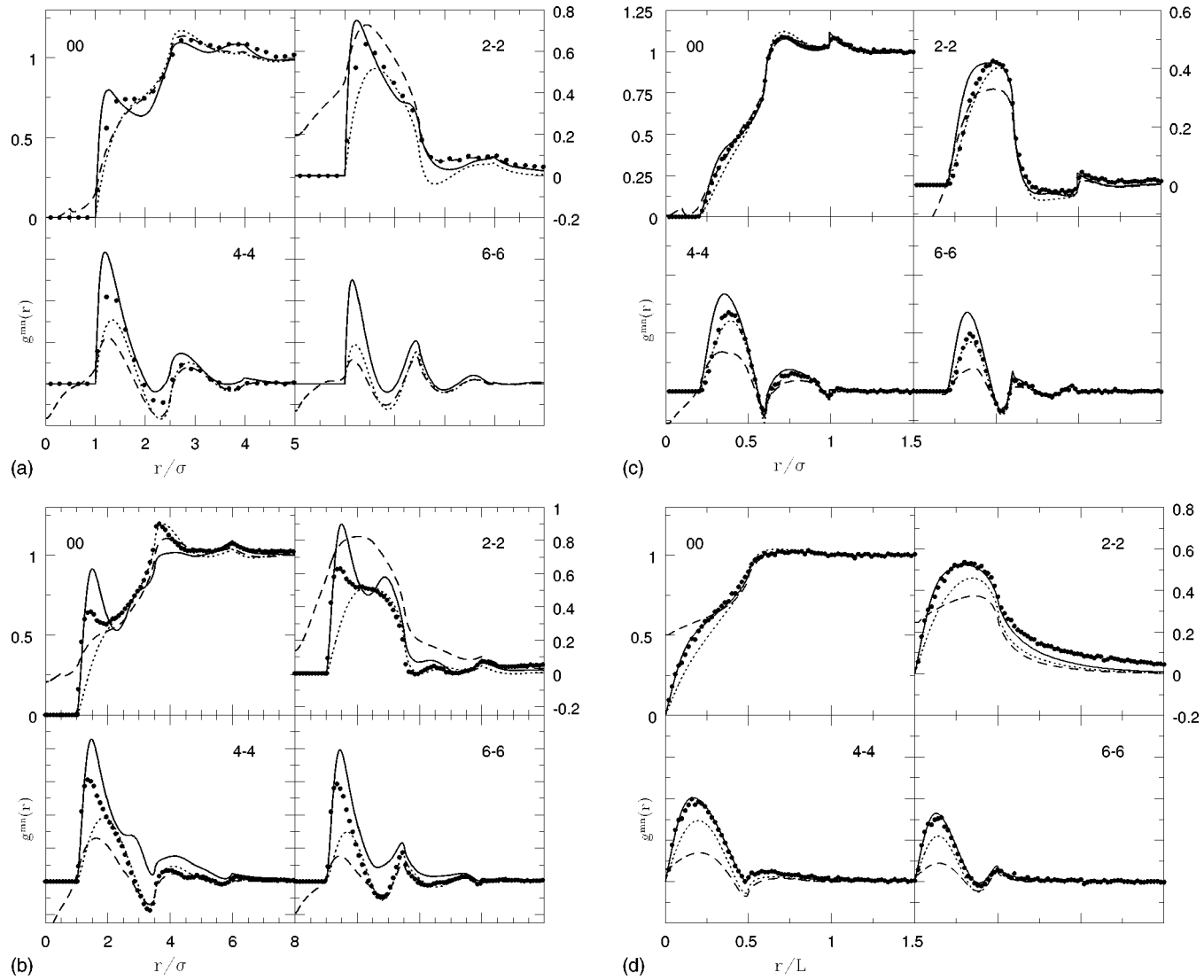

FIG. 4. (a) Pair correlation expansion coefficients $g^{mn}(r)$ of the pair correlation function for the hard ellipse fluid of aspect ratio $\kappa=4$ at the density $\rho^*=0.152$. The solid line is for the first approximation, the dotted line for the HNC theory, and the dashed line for the PY theory. The dots are simulation results from Ref. [5]. The projection indices (m,n) are indicated on the corresponding panels. The vertical labeling is the same for projections g^{2-2}, g^{4-4}, and g^{6-6}. (b) Expansion coefficients $g^{mn}(r)$ of the pair correlation function for the hard diskorectangle fluid for $L^*=5$ at the density $\rho^*=0.078$. The lines are the same as in (a). (c) Expansion coefficients $g^{mn}(r)$ of the pair correlation function for the hard cut disk fluid for $d^*=0.2$ at the density $\rho^*=1.5$. The lines are the same as in (a). (d) Expansion coefficients $g^{mn}(r)$ of the pair correlation function for the hard needle fluid at the density $\rho^*=2.5$. The lines are the same as in (a) and the filled circles are our computer simulation results.

that the PY theory had no solutions for densities above $\rho^*=1.59$. This is sufficient, however, to point out the particularities of this fluid. First, we observe the same features of the geometrical approach as observed in Figs. 4(a) and 4(b). The PY results are in better agreement with the simulations than any of the two other results, except for g^{00} near $r^*=0.35$. One sees also that none of the angular components develop long-range correlations at this density. The short-range cubic-type ordering that is particular to the thickness $d^*=0.2$ is already visible at this density, particularly in the $g^{2-2}(r)$ component, which shows a first broad peak indicating a piling of two cut disks. Then one observes a large negative small peak, indicating a perpendicular ordering of another short stack pile of two cut disks. This is corroborated by the $g^{4-4}(r)$ component, which has a positive second peak. These tendencies develop strongly at higher densities, indicating clearly that there is a cubatic-type ordering at least in the short-range region. This picture is also supported by the snapshots that show a typical ''broken book pile'' picture with the short stack piles being locally perpendicular to each other. This picture is not seen at larger $(d^*=0.5)$ or lower $(d^*=0.1)$ thicknesses. The question whether or not this type of order is long ranged is difficult to answer mainly in the two-dimensional systems where any long-range order is plagued by defect formations and bindings. We leave this question open until further dedicated studies.

Finally, the hard needle case is shown in Fig. 4(d). We recall that here the geometrical approach predicts that the DCF is equal to the Mayer function and thus is independent of the density. The only density dependence of the corresponding pair correlation comes through the OZ equation, thus explaining the very weak density dependence observed

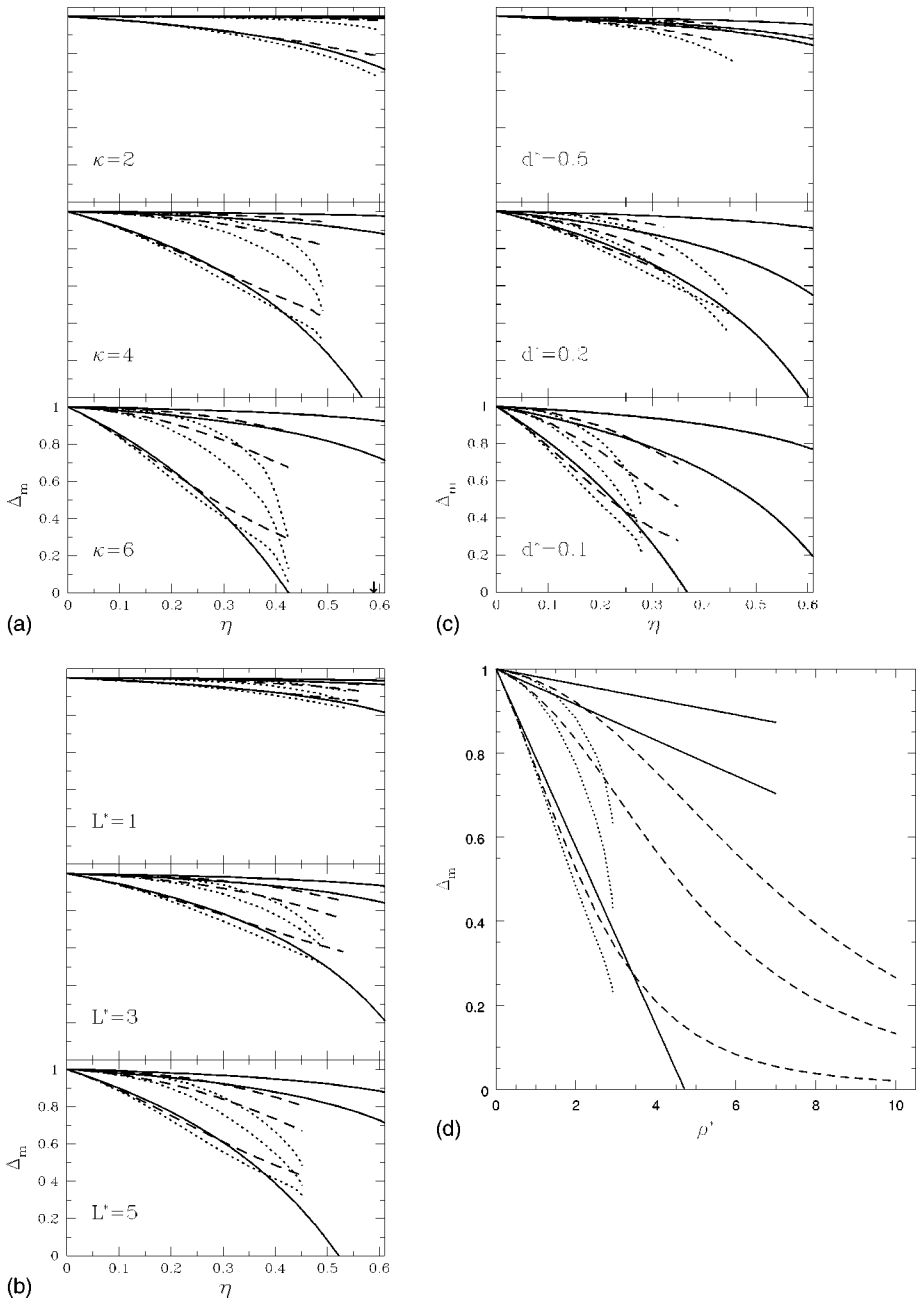

FIG. 5. (a) Orientational instability factors $\Delta_m(m=2,\ 4,$ and 6) versus the packing fraction $\eta=\rho S$ for the hard ellipse fluids of aspect ratios $\kappa=2,\ 4,$and 6. The solid lines are for the first approximation of the DCF and the dotted lines and dashed lines correspond, respectively, to the HNC and PY theory results. For each of the theories, the topmost curve is for $m=6$ and the lowermost for $m=2$. The arrows indicate the isotropic-nematic transition densities as found by the computer simulations (Ref. [2]). (b) Orientational instability factors Δ_m for the hard diskorectangle fluids for $L^*=1,\ 3,$ and 5. The lines are the same as in (a). (c) Orientational instability factors Δ_m for the hard cut disk fluids for $d^*=0.5,\ 0.2,$ and 0.1. The lines are the same as in (a). (d) Orientational instability factors Δ_m for the hard needle fluid. The lines are the same as in (a).

in Fig. 4(d). The HNC result are surprisingly accurate, which is true for all densities for which this theory could be solved. This finding is in agreement with the good results obtained for the pressure.

C. Orientational instability of the isotropic phase

The Δ_m for all three type of fluids are displayed in Figs. 5(a)–5(c). Only the first approximation for the DCF was retained here, as the second one predicts instabilities at densities far too low, due to the fact that the χ_0 coefficient in Eq. (28) for the second approximation is too large (see Fig. 1) compared to that of the first approximation. The isotropic-nematic instability functions Δ_m for the hard ellipse fluids are plotted in Fig. 5(a) versus the packing fraction $\eta=\rho S$ (S is the surface of the ellipse) for the three aspect ratios $\kappa=2,\ 4,$ and 6. The HNC and PY results are also shown, respectively, as dotted and dashed lines. The instability density is the solution of $\Delta_m=0$. Usually, for $m=2$ such a solution indicates an orientational instability towards the nematic order. For higher m values more complex ordering tendencies could be destabilizing the isotropic phase. The

case of the integral equation is more complex. The Δ_m from the solution of these equations stops before the zero value is attained because no numerical solution is found beyond a certain value of the density. The reason why the solution is lost is not clearly known. Such behavior is also met in other cases such as liquid-gas coexistence [23] or Coulombic fluids [24]. It is important to note that the loss of the numerical solutions is totally independent of the accuracy of the algorithm used in each case and is believed to stem from the mathematical nature of the PY and HNC closures [23]. It is customary to consider that the extrapolation of Δ_2 to zero gives the density at the limit of stability of the isotropic phase.

We recall that computer simulations of Cuesta and Frenkel [2] for the same fluids have shown the existence of an isotropic-nematic transition only for ellipses of aspect ratios 4 and 6. It is obvious from Fig. 5(a) that the fluid of ellipse for $\kappa=2$ has no orientational instabilities (the Δ_2 curves extrapolate to zero beyond $\eta=1$). For the $\kappa=4$ and $\kappa=6$ cases we note that both HNC and the geometrical approach indicate an orientational instability towards the nematic phase and at densities quite close to each other. These values are much smaller than those predicted by computer simulations. We find here that in the case of $\kappa=4$, $\eta_{ins}=0.567$ for the geometrical approach, while the computer simulation predict $\eta_{IN}\approx 0.74$. Similarly, for $\kappa=6$ we find $\eta_{ins}=0.424$, while the simulations predict $\eta_{IN}\approx 0.59$. We note, however, that the analysis of the computer simulations is based on the apparition of defects binding phenomena, which are not accounted for in the theories discussed here. The comparison with other approaches such as density functional theories [25] shows that the instability densities predicted here are larger than those found in such approaches, which makes the present approach even more appealing. In particular, such approaches generally predict transitions for all aspect ratios, a feature that is unrealistic. As noted in Ref. [5], the PY theory predicts no orientational instabilities (or at unreasonably high-density values), a feature already observed in three dimensions [26]. We note another feature that was also observed in previous studies: The HNC theory predicts orientational instability from all $\Delta_m=4$ at the same density. This feature is almost a signature of the HNC behavior for anisotropic fluids.

We turn now to the fluids of diskorectangles. Figure 5(b) shows features similar to those of Fig. 5(a). We note that for diskorectangles of aspect ratio $\kappa=4$ the geometrical theory predicts an instability at $\eta_{ins}=0.663$. However, in this case, the curvature of the Δ_2 function from the HNC theory does not allow an unambiguous extrapolation to zero. In fact, the analysis of the long-distance behavior of $h^{2-2}(r)$, which is responsible for the orientational destabilization of the isotropic phase, shows that in this case the function has no long-range tail. Thus the HNC theory does not predict an orientational instability. This seems to be in accord with our computer simulations, where we could not stabilize a nematic phase at high densities. For the case $\kappa=6$ the geometrical approach predicts $\eta_{ins}=0.521$. Similarly to the previous case, the extrapolation to zero of the Δ_2 curve from the HNC theory cannot be obtained accurately. In accord with this latter finding, our computer simulation could not find a stable nematic phase. The nematic phase seems to appear for aspect ratios larger than $\kappa=7$. We could observe unambiguously such a phase for $\kappa=8$. This particular fluid certainly deserves a more thorough study in the future. Indeed, our finding supports the idea that fluids of hard diskorectangles have a stable nematic phase for particle aspect ratio larger than that needed for the case of fluids of a hard ellipse. This offers some similarities to the three-dimensional case, where the nematic phase for spherocylinders was observed for aspect ratios larger than those for ellipsoids [27].

The fluid of hard cut disks also has interesting features. Figure 5(c) shows again that the geometrical approach predicts nematic-type orientational instabilities for thicknesses $d^*=0.2$ and $d^*=0.1$ (aspect ratios of 5 and 10, respectively). However, the HNC integral equation shows a curious crossover of Δ_2 and Δ_4 at thicknesses $d^*=0{,}2$, which is very much reminiscent of that observed for the cubatic ordering in three dimensions [18]. The confirmation by computer simulation of the existence of such an order in the two-dimensional case is beyond the scope of this work, mainly because the phase transitions in two dimensions are plagued by the defect binding phenomena, which make the small-scale studies very cumbersome. However, snapshots from our computer simulation studies [28] reveal that a cubatic-type order exists, at least locally, as one observes a broken book pile type of picture, with short piles being locally perpendicular to each other. This type of order is not visible for larger ($d^*=0.5$) or smaller ($d^*=0.1$) thicknesses. For $d^*=0.2$, the analysis of the long-range part of $h^{4-4}(r)$ shows that this function has a long-range part growing faster than $h^{2-2}(r)$. As our simulations are performed for at most 200 particles, it is difficult to speak of long-range behavior. However, this analysis support the short- to medium-range picture observed in the snapshots.

It is interesting to ask whether the geometrical theory can predict such an instability. In view of Eq. (28), a simple investigation of the Mayer function expansion coefficients $\tilde{f}_M^{m-m}(k=0)$ is sufficient. In Fig. 6 we have plotted such values for $m=0$, 2, 4, and 6 versus the thickness d^*. One sees that for $d^*\geqslant 0.44$ the geometrical approach will predict the cubatic ordering. For $d^*\geqslant 0.61$ one will eventually observe $\Delta_6=0$ before the other two modes. A similar feature was also observed for cut spheres [18] where the geometrical approach also predicted cubatic ordering for unrealistic large thicknesses. We find finally that the PY theory predicts again no orientational instabilities.

We now examine briefly the case of the hard needle fluid in Fig. 5(d). Clearly the HNC theory predicts a nematic instability at the density $\rho/L\approx 3$, whereas the geometrical theory predicts the same type of instability at exactly the Onsager density $\rho/L=4.71$. This last point is no surprise since the geometrical DFC is reduced to the Mayer function in this limit. The linearity of all the modes Δ_m with respect to the density is also a direct consequence of this feature [see Eq. (28)]. We note that, in the case of the HNC theory *all* the modes seem to point to the same instability density. This is a typical feature of the HNC theory. The PY theory, however, shows a very different concavity for all the modes Δ_m, and even if very small values of the mode Δ_2 can be achieved, it is not possible to conclude any solution for the orientational instability $\Delta_2=0$. Similarly to the case of the hard platelet

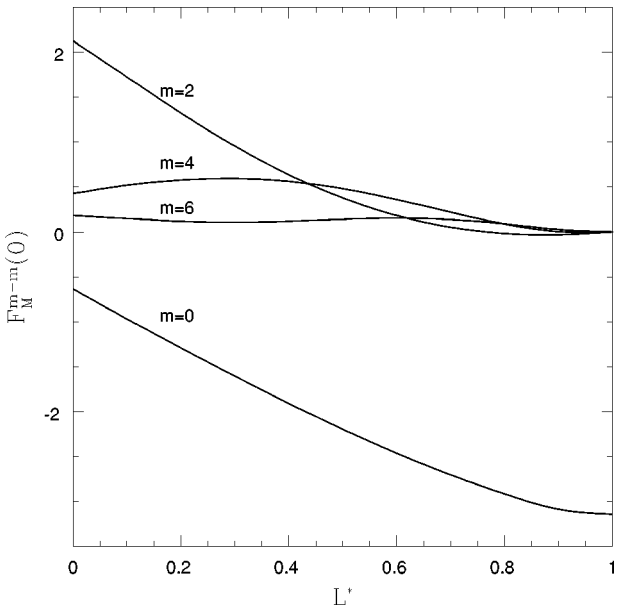

FIG. 6. $k=0$ values of the Fourier-Bessel transforms of the Mayer function expansion coefficients $\tilde{f}_M^{m-m}$ for the hard cut disk fluid, versus the cut disk thickness d^*. The different m values are indicated next to the corresponding curves. Note that the $m\neq 0$ values are multiplied by 10.

fluid in three dimensions, this extreme example of a two-dimensional fluid can serve as a test of the theories [22]. In the present case, one sees that the HNC and PY theories have a similar low-density behavior, which is very different for the geometrical DCF results. One is then tempted to say from Eq. (28) that the density-dependent factor χ_0 is not correctly accounted for by the approximations described here. This remark opens a route for systematic corrections of the geometrical approach [22].

IV. DISCUSSION AND CONCLUSION

From Sec. III it seems quite clear that the geometrical approach to the DCF and the thermodynamic properties for two-dimensional fluids of hard bodies can be successfully applied for moderate aspect ratios and densities and to a lesser extent for larger densities and aspect ratios as well. It is important to note that the pair DCF is not entirely written as a sum of convolution of weight functions, due to the fact that it contains the true Mayer function. The latter cannot be written as a convolution of weight functions, except for few very special cases, such as hard disks or rigidly parallel particles [16]. Although being PY-like by construction, the geometrical DCF also has some desirable features from the HNC theory, such as the prediction of the orientational instability, a feature totally absent from the PY theory. Moreover, this approach is numerically simpler than the integral approaches, an additional attractive feature to bear in mind in the case of application to more complex systems, such as mixtures and solid-liquid interfaces for example. Indeed, the present approach allows the calculation of a particular expansion coefficient $c^{mn}(r)$ without having to compute the full DCF or the pair correlation function. In this way, one could simply extract the desired orientational properties, such as $c^{2-2}(r)$, the component of the DCF responsible for the orientational instability.

However, the geometrical theory fails to account for the ordering features in the sense that it always predict an orientational instability of the isotropic phase at a density too small. This feature, which was already true in the three-dimensional case, seems worse in two dimensions. It could be explained by the fact that the ordering in two dimensions is strongly influenced by defects, a feature that is not accounted for in the theory developed herein.

The present work raises some questions about the diagrammatic nature of the three theories compared herein. The DCF as expressed by Eq. (6) contains only pair terms. All the higher-order density correlations are contained in the χ_α coefficients. In view of the poor agreement observed for very anisotropic particles or oblate shapes, one is led to think that more than pair correlations must be incorporated in the spatial-variable-dependent factors. This is particularly true when examining the case of hard cut disk fluids as well as the three-dimensional case of cut spheres [18]. In order to describe the short-range cubatic-type piling effect one must account for more than three particle correlations. Clearly, the HNC theory does so (also true in three dimensions [18]). The case of the PY theory is more complex. Indeed, the PY DCF contains the Mayer function in the low-density limit expansion, as it gives the correct second and third virial coefficients. One would then expect this theory to predict the cubatic ordering, at least for large thicknesses. This, however, is not the case (not even in three dimensions [18]). So the higher-order density expansion terms of the PY DCF must somehow destroy the effect of the Mayer function. This argument is even more true when examining the simpler case of the nematic instability, which is also contained in the Mayer function (at an Onsager level of approximation for example) and consequently in the geometrical DCF, but not in the PY DCF. It would be of fundamental interest to find, at a diagrammatic level, why the geometrical approach, although simpler than the PY approximation, provides a better description of anisotropic fluids, in closer agreement with the HNC theory. In particular, it is interesting to know whether correcting the geometrical DCF in order to account for a zero pair correlation inside the hard core might increase or decrease the accuracy of this method. The systematic study of extreme models such as the hard needles or the hard platelets by these theories also helps answer some of the unanswered questions. These answers in turn might help shed some light on the criticality of the two integral equation theories, a subject that has recently gained renewed interest.

APPENDIX A: WEIGHT FUNCTIONS

In what follows we give the formal expression for the expansion coefficients of the surface weight $w^{(s)}(1)$ and the line weight $w^{(l)}(1)$, which are essential for the development of our theory. The expressions are restricted to particles having a uniaxial symmetry because all the convex objects studied here have the same symmetry. We recall that $w^{(\alpha)}(1)=w^{(\alpha)}(\mathbf{r},\mathbf{u})$, where $\mathbf{u}$ is the orientation of the molecule and $\mathbf{r}$ is the radial vector to the surface of the particle. First we develop the weights in the general basis set of rotational invariants Eq. (15). One has, using the simplified no-

tation $w_m^{(\alpha)} \equiv w_{m0}^{(\alpha)}$, an expansion identical to that of Eq. (9),

$$w^{(\alpha)}(1) = w^{(\alpha)}(\mathbf{r},\mathbf{u}) = \sum_m w_m^{(\alpha)}(r)\Psi^{m0}(\theta_r,\theta_1), \quad \text{(A1)}$$

where $\Psi^{m0}(\theta_r,\theta_1) = \exp(im\theta)$ and $\theta = \theta_1 - \theta_r$. We see that the weight functions depend only on the relative angle between **r** and **u**. Using the orthogonality of the invariants one can invert this relation to get the $w_m^{(\alpha)}(r)$,

$$w_m^{(\alpha)}(r) = \frac{1}{2\pi}\int d\theta\, w^{(\alpha)}(r,\theta)\Psi^{m0}(\theta). \quad \text{(A2)}$$

When the definitions of Eq. (13) are introduced in Eq. (A2) one gets the desired expansion coefficients. Because the weight functions are distributions, some care should be taken before performing the angular integration. In all the results below $R(\theta)$ represents the distance from the center of the particle to its surface and θ is the angle between the symmetry axis of the particle and **R**. For all the convex objects studied in the present work $R(\theta)$ is a simple analytical function of the angle θ and the reciprocal function $\theta(R)$ is easily obtained (see Appendix B).

For the surface weight, $w^{(S)}(r,\theta) = H(r,\theta) \equiv H(R(\theta) - r)$, where $H(x)$ is the Heaviside step function, which is unity only for $x \geqslant 0$. Using the symmetry properties of the particle, the integral in Eq. (A2) can be performed to give

$$w_m^{(S)}(r) = \frac{2}{\pi}\theta(R) j_0(m\theta(R)), \quad \text{(A3)}$$

where $j_0(x)$ is the zeroth-order spherical Bessel function.

The line weight is more delicate as it involves a δ function. In this case, $w^{(L)}(r,\theta) = t(r,\theta)\,\delta(R(\theta) - r)$, where $\delta(x)$ is the Dirac distribution and the function $t(r,\theta) = \sqrt{1 + (1/r^2)\,(dr/d\theta)^2}$. The integral in Eq. (A2) can be evaluated by making the formal variable change $r \to \theta(r)$. After some algebra one finds

$$w_m^{(L)}(r) = \frac{2}{\pi}\frac{t(r,\theta(R))\cos[m\theta(R)]}{dR/d\theta}, \quad \text{(A4)}$$

where it is understood that the substitution $r = R$ must be done after the calculations involving $R(\theta)$ are done.

Appendix B gives explicit expressions for the weights for the particles studied in this work. The convolution products in Eq. (18) are evaluated through the numerical Fourier-Bessel transforms of the weights as evaluated above. In the case of the line weight, integrable divergence may appear at the R values corresponding to the angle $\theta = 0$ and/or $\theta = \pi/2$. They simply correspond to the properties of the slope $dR/d\theta$ at these points and are found for particles such as the hard ellipse or the diskorectangle. These divergences are handled exactly by considering the Fourier-Bessel transforms of the integral of the line weights, which are well defined functions [16]. The explicit relation linking the Fourier-Bessel transform of the line weight $w_m^{(L)}(r)$ and its integral $W_m^{(L)}(r)$ is

$$\tilde{w}_m^{(L)}(k) = -ik\mathcal{T}_{m+1}[W_m^{(L)}] - (m+1)\mathcal{T}_m\left[\frac{W_m^{(L)}}{r}\right], \quad \text{(A5)}$$

where $\mathcal{T}_m(F)$ is the Fourier-Bessel transform of order m of the function $F(r)$ [5,29].

APPENDIX B: WEIGHT FUNCTIONS FOR FEW 2D CONVEX BODIES

The surface and line weights, together with the SPT geometrical parameters (surface S and perimeter $\mathscr{l}$), are given herein. Both weight functions can be expressed as

$$w_m^{(S)}(r) = \frac{2}{\pi}\theta(r)\dot{j}_0(m\theta(r)), \quad \text{(B1)}$$

$$w_m^{(L)}(r) = \nu(r)\cos[m\theta(r)], \quad \text{(B2)}$$

where $\dot{j}_0$ is the zeroth-order spherical Bessel function. The functions $\theta(r)$ and $l(r)$ are specific to each convex bodies. All the distance units are reduced with respect to the diameter σ of the disk to which each of the convex bodies goes in the spherical limit.

1. The hard ellipse

For the aspect ratio κ one has $S = \pi/4\kappa$ and $\mathscr{l} = 2\kappa\int_0^{\pi/2} d\gamma\sqrt{\cos^2(\gamma) - \sin^2(\gamma)/\kappa^2}$,

$$\theta(r) = \arccos\left[\frac{\kappa}{\sqrt{\kappa^2-1}}\sqrt{1 - \frac{1}{4r^2}}\right], \quad \text{(B3)}$$

$$\nu(r) = \frac{4}{\pi}\sqrt{\frac{1 + \kappa^2 - 4r^2}{(4r^2-1)(\kappa^2-4r^2)}}. \quad \text{(B4)}$$

2. The hard diskorectangle

For the rectangle length L (aspect ratio $\kappa = L+1$), one has $S = \pi/4 + L$ and $\mathscr{l} = \pi + 2L$. The expressions for the weights depend on the disk or rectangle parts. For $1 \leqslant r \leqslant \sqrt{L^2+1}/2$ one has

$$\theta(r) = \arccos\sqrt{1 - \frac{1}{4r^2}}, \quad \text{(B5)}$$

$$\nu(r) = \frac{2}{r}\sqrt{\frac{5r^2-1}{4r^2-1}}, \quad \text{(B6)}$$

and for $\sqrt{L^2+1}/2 \leqslant r \leqslant (L+1)/2$ one has

$$\theta(r) = \arccos\left(\frac{4r^2 + L^2 - 1}{4rL}\right), \quad \text{(B7)}$$

$$\nu(r) = \frac{8}{\pi}\frac{1}{\sqrt{[4r^2 - (L+1)^2][(L-1)^2 - 4r^2]}}. \quad \text{(B8)}$$

3. The hard cut disk

For the cut disk thickness d (aspect ratio $\kappa=1/d$) one has $S=\pi/4-(1/2)\arctan(\sqrt{1/d^2-1})+(d/2)\sqrt{1-d^2}$, $\ell=\pi-2\arctan(\sqrt{1/d^2-1})+2\sqrt{1-d^2}$,

$$\theta(r)=\frac{\pi}{2}-\arccos\left(\frac{d}{2r}\right), \tag{B9}$$

$$\nu(r)=\frac{4}{\pi\sqrt{4r^2-d^2}}. \tag{B10}$$

[1] S. Chandrasekar, *Liquid Crystals* (Cambridge University Press, Cambridge, 1992).
[2] J. A. Cuesta and D. Frenkel, Phys. Rev. A **42**, 2126 (1990).
[3] J. A. Cuesta, C. F. Tejero, and M. Baus, Phys. Rev. A **39**, 6498 (1989).
[4] D. A. Ward and F. Lado, Mol. Phys. **63**, 623 (1988).
[5] P. G. Ferreira, A. Perera, M. Moreau, and M. M. Telo da Gama, J. Chem. Phys. **95**, 7591 (1991).
[6] K. J. Strandburg, Rev. Mod. Phys. **60**, 161 (1988).
[7] F. F. Abraham, Phys. Rep. **80**, 339 (1981).
[8] M. Kosterlitz and D. Thouless, J. Phys. C **6**, 1181 (1973).
[9] J. P. Hansen and I. R. McDonald, *Theory of Simple Liquids* (Academic Press, London, 1986).
[10] E. Leutheusser, Physica A **124**, 667 (1984).
[11] Y. Rosenfeld, Phys. Rev. Lett. **63**, 980 (1989); Y. Rosenfeld, D. Levesque, and J. J. Weis, J. Chem. Phys. **92**, 6818 (1990).
[12] Y. Rosenfeld, Phys. Rev. A **42**, 5978 (1990).
[13] A. Chamoux and A. Perera, J. Chem. Phys. **104**, 1493 (1996).
[14] A. Kloczkowsky and J. Stecki, Mol. Phys. **46**, 13 (1982).
[15] A. Chamoux and A. Perera, Mol. Phys. **93**, 649 (1998).
[16] A. Chamoux, Ph.D. thesis, Université Pierre et Marie Curie, 1997 (unpublished).
[17] J. A. C. Veerman and D. Frenkel, Phys. Rev. A **41**, 3237 (1990).
[18] A. Chamoux and A. Perera, J. Chem. Phys. **108**, 8172 (1998).
[19] J. F. Lutsko and M. Baus, Phys. Rev. A **41**, 6647 (1990).
[20] M. P. Allen, C. P. Mason, E. de Miguel, and J. Stelzer, Phys. Rev. E **52**, R25 (1995); J. Stelzer, L. Longa, and H. H. Treblin, in Proceedings of the 15th International Liquid Crystal Conference, Budapest, 1994 [Mol. Cryst. Liq. Cryst. Sci. Technol., Sect. A **262**, 455 (1995)].
[21] D. Frenkel and R. Eppenga, Phys. Rev. A **31**, 1776 (1985).
[22] A. Chamoux, A. Perera, and P. G. Ferreira (unpublished).
[23] P. G. Ferreira, R. L. Carvalho, M. M. Telo da Gama, and A. G. Schlijper, J. Chem. Phys. **101**, 594 (1993).
[24] L. Belloni, J. Chem. Phys. **98**, 8080 (1993).
[25] J. A. Cuesta, C. Tejero, Hong Xu, and M. Baus, Phys. Rev. A **44**, 5306 (1991).
[26] A. Perera, P. G. Kusalik, and G. N. Patey, J. Chem. Phys. **87**, 1295 (1987).
[27] P. Bolhuis and D. Frenkel, J. Chem. Phys. **106**, 666 (1997).
[28] A. Chamoux and A. Perera (unpublished).
[29] J. D. Talman, J. Comput. Phys. **29**, 35 (1978).